UNIVERSITY OF AMSTERDAM

UvA-DARE (Digital Academic Repository)

Passive Irradiated Circumstellar Disks with an Inner Hole

Dullemond, C.P.; Dominik, C.; Natta, A.

Published in:
Astrophysical Journal

DOI:
10.1086/323057

Link to publication

Citation for published version (APA):
Dullemond, C. P., Dominik, C., & Natta, A. (2001). Passive Irradiated Circumstellar Disks with an Inner Hole. Astrophysical Journal, 560, 957-969. DOI: 10.1086/323057

General rights
It is not permitted to download or to forward/distribute the text or part of it without the consent of the author(s) and/or copyright holder(s), other than for strictly personal, individual use, unless the work is under an open content license (like Creative Commons).

Disclaimer/Complaints regulations
If you believe that digital publication of certain material infringes any of your rights or (privacy) interests, please let the Library know, stating your reasons. In case of a legitimate complaint, the Library will make the material inaccessible and/or remove it from the website. Please Ask the Library: http://uba.uva.nl/en/contact, or a letter to: Library of the University of Amsterdam, Secretariat, Singel 425, 1012 WP Amsterdam, The Netherlands. You will be contacted as soon as possible.

UvA-DARE is a service provided by the library of the University of Amsterdam (http://dare.uva.nl)

Download date: 20 Oct 2017

THE ASTROPHYSICAL JOURNAL, 560:957–969, 2001 October 20
© 2001. The American Astronomical Society. All rights reserved. Printed in U.S.A.

PASSIVE IRRADIATED CIRCUMSTELLAR DISKS WITH AN INNER HOLE

C. P. DULLEMOND
Max Planck Institut für Astrophysik, Postfach 1317, D-85741 Garching, Germany; dullemon@mpa-garching.mpg.de
C. DOMINIK
Sterrenkundig Institut "Anton Pannekoek," Universiteit van Amsterdam, Kruislaan 403, SJ NL-1098 Amsterdam, Netherlands; dominik@astro.uva.nl
AND
A. NATTA
Osservatorio Astrofisico di Arcetri, Largo E. Fermi 5, I-50125 Firenze, Italy; natta@arcetri.astro.it
Received 2001 March 14; accepted 2001 June 26

ABSTRACT

A model for irradiated dust disks around Herbig Ae stars is proposed. The model is based on the flaring disk model given by Chiang and Goldreich in 1997, but with the central regions of the disk removed. The inner rim of the disk is puffed up and is much hotter than the rest of the disk because it is directly exposed to the stellar flux. If located at the dust evaporation radius, its reemitted flux produces a conspicuous bump in the spectral energy distribution (SED) that peaks at 2–3 μm. We propose that this emission is the explanation for the near-infrared bump observed in the SEDs of Herbig Ae stars. We study for which stellar parameters this bump would be observable and find that it is the case for Herbig Ae stellar parameters but not for T Tauri stars, confirming what is found from the observations. We also study the effects of the shadow cast by the inner rim over the rest of the flaring disk. The shadowed region can be quite large, and under some circumstances the entire disk may lie in the shadow. This shadowed region will be much cooler than an unshadowed flaring disk, since its only heating sources are radial radiative diffusion and possible indirect sources of irradiation. Under certain special circumstances the shadowing effect can suppress, or even completely eliminate, the 10 μm emission feature from the spectrum, which might explain the anomalous SEDs of some isolated Herbig Ae stars in the recent sample of Meeus and colleagues. At much larger radii the disk emerges from the shadow and continues as a flaring disk toward the outer edge. The emission from the inner rim contributes significantly to the irradiation of this flaring disk. The complete semianalytical model, including structure of the inner edge, the shadowed region, and the flared outer part, is described in detail in this paper, and we show examples of the general behavior of the model for varying parameters.

Subject headings: circumstellar matter — infrared: stars — stars: emission-line, Be

1. INTRODUCTION

The hypothesis that Herbig Ae/Be (HAeBe) stars (Herbig 1960) are intermediate-mass pre–main-sequence stars is today generally accepted. The large infrared (IR) excess observed from these stars can be naturally explained in this context by emission from a protostellar/protoplanetary disk. This picture has been given more credibility in recent years by interferometric observations at millimeter wavelengths (Mannings & Sargent 1997, 2000). Over the years, various disk models have been proposed for pre–main-sequence stars, among which are disks powered by accretion (Lin & Papaloizou 1980; Bell & Lin 1994), irradiated nonaccreting (passive) disks (Kenyon & Hartmann 1987; Chiang & Goldreich 1997, hereafter CG97), and irradiated accretion disks (Ruden & Pollack 1991; Calvet et al. 1991, 1992; D'Alessio et al. 1998, 1999; Bell 1999). The spectral energy distributions (SEDs) of Herbig Ae stars seem to be best fitted by passive irradiated flaring disks, at least at mid- and far-IR wavelengths (Chiang et al. 2001). At near-IR (NIR) wavelengths, however, the flaring disk picture fails to agree with the observed SEDs. The same problem is encountered when fitting nonirradiated accretion disk models to the SEDs. Hillenbrand et al. (1992) noticed that in 29 out of 51 HAeBe stars (their group I sources) the SED at NIR and mid-IR wavelengths was well fitted by models of geometrically flat, optically thick disks with very large accretion rates, but that these disks needed to be optically thin in their inner parts, to account for the distinctive inflection shown by all HAeBe stars at $1.2 \lesssim \lambda \lesssim 2.2$ μm (see also Lada & Adams 1992). Better measured SEDs for a number of HAeBe stars of spectral type A (hereafter HAe) have confirmed the Hillenbrand et al. (1992) results.

All the observed isolated HAe stars have large NIR emission in excess of the photospheric one with very similar dependence on wavelength, which can be described as an NIR "bump": the excess monochromatic luminosity νF_ν is negligible around 1 μm, peaks around 2 μm, and decreases slowly with wavelength to about 8 μm, where the silicate emission feature starts (Meeus et al. 2001; Natta et al. 2001). These stars have very little extinction, so that reddening in the NIR is negligible.

The negligible opacity of the inner disk region, required to explain the NIR bump, is not consistent with the high accretion rates necessary to account for the large NIR excess, as discussed by Hartmann, Kenyon, & Calvet (1993). These authors suggested that, given the difficulties of applying disk models to HAeBe stars, one should consider the hypothesis that the emission originates in a dusty circumstellar envelope, possibly containing very small grains transiently heated by ultraviolet photons. This possibility, however, has been ruled out by theoretical models (Natta & Krügel 1995) and by *Infrared Space Observatory* (*ISO*) observations (Meeus et al. 2001).

An alternative explanation for the NIR behavior of HAe

stars has recently been proposed by Natta et al. (2001). Their model starts from the notion that the mid- and far-IR excess of HAe stars can be well fitted with a passive irradiated flaring disk, as was mentioned above.

As expected, these models fail to explain the observations in the NIR. However, Natta et al. (2001) have noticed that, if one truncates the flaring disk at a certain radius (i.e., introduces a hole), the emission from the inner rim of this disk is nonnegligible. This inner rim will have a considerable covering fraction around the star, and it will acquire a temperature much hotter than what the flaring disk interior at the same radius would have. This is because the flaring disk receives the stellar radiation under a small grazing angle and will therefore be relatively cool, while the inner rim is in full sight of the star and will therefore be hot. In fact, if one assumes that the inner edge of the disk is naturally located at the radius where dust grains acquire their evaporation temperature, then the emission from this inner rim is going to produce an NIR bump very reminiscent of the observed one in shape and intensity.

In this paper we wish to proceed further along this path and investigate a number of issues that have not been addressed by Natta et al. (2001). First, we formalize the description of the structure of a disk with a large inner radius, using the flaring disk models of CG97 as a starting point. In particular, we wish to investigate how the presence of the hot inner rim modifies structure and appearance of the rest of the disk. Since the inner rim is much hotter than the CG97 disk at the same radius, its vertical scale height will be larger as well. In other words, the inner rim of the disk will puff up. This will enhance the NIR emission but also cast a shadow over the disk behind it. Part of the disk that would normally be directly illuminated by the stellar radiation will now be in the shadow and therefore collapse and cease to emit IR radiation. At large enough radii, it is possible that the flaring shape of the CG97 disks will be conserved and that the disk will grow out of the shadow, unchanged by the presence of the rim. We thus propose a scenario in which the emission from the reprocessing disk comes from a hot inner rim, caused by dust evaporation, plus the nonshadowed part of a truncated CG97 disk.

A second point we discuss concerns the behavior of the NIR emission as a function of the spectral type of the star. The IR spectra of T Tauri stars (TTSs) are well described by disk models with small or zero inner holes (Beckwith et al. 1990; Kenyon, Yi, & Hartmann 1996) and moderate accretion rates (Gullbring et al. 1998). The few known pre–main-sequence stars of spectral type F and G seem closer in properties to TTSs than to HAe stars (Hillenbrand et al. 1992; Hartmann et al. 1993). We show that this behavior can be explained by the same disk models and that it is caused by a combination of effects. First of all, the relative importance of the NIR bump emission from the inner edge in comparison to the disk emission is smaller for stars of later spectral type. Secondly, the stellar atmospheric spectrum shifts toward longer wavelengths as the effective temperature of the star decreases, swamping the rim emission. Finally, it is possible that TTSs have on average higher accretion rates, and therefore more optically thick inner disks, than HAe stars.

The structure of the paper is as follows. In § 2 we discuss the equations, and in § 3 we describe how the SED is computed. The results are presented in § 4, and we conclude with a discussion in § 5.

2. THE STRUCTURE OF A DISK WITH A LARGE INNER HOLE

In this section we derive the equations governing the structure of a passively irradiated circumstellar disk with an inner hole. The main effect of the inner hole on the disk structure is a vertical boundary that is irradiated directly by the star, heating it to temperatures higher than what would be expected at the same location for a thin disk with grazing irradiation only. Because of the higher temperature, the disk boundary will be puffed up, and the material immediately outside the inner rim will be shadowed, leading to a decreasing scale height. At large distances from the star it is possible that the disk becomes high enough to emerge from the shadow of the inner rim, in which case it may continue to flare like a disk without a puffed-up inner rim. However, it is not certain that the disk will be able to leave the shadow. This is a dynamical question, and the answer may depend upon the history of the disk and many other parameters (e.g., was the disk flaring when the inner boundary started to emerge and to puff up?).

Figure 1 shows our scenario, where we assume that the flared part of the disk exists when it can. We divide the disk structure calculations into three parts (inner rim, shadowed region, and flared component) and derive the basic equations governing the structure in the three regions. We start with the well-known flared part.

2.1. *Flaring Disk*

For the flaring part of the disk we follow the line of CG97 with some minor modifications. For completeness, and in order to introduce the nomenclature, we repeat the basic equations without physical discussion.

2.1.1. *Disk Interior*

Direct stellar radiation impinges onto the disk at an angle α given by $\alpha = 0.4R_*/R + R\,d(H_{cg}/R)/dR$, where R_* is the radius of the star, R the distance from the star in the disk plane, and H_{cg} the height of the disk photosphere above the midplane. Anticipating a nearly power-law behavior, we replace Rd/dR by $\gamma - 1$, where γ is a slowly varying function of the order of 9/7. We can thus rewrite the expression for α as

$$\alpha = \frac{0.4R_*}{R} + (\gamma - 1)\,\frac{H_{cg}}{R}\,. \tag{1}$$

The $(\gamma - 1)$ factor is self-consistently determined as a function of R, using a numerical method devised by Chiang et al. (2001). In this way energy conservation is ensured, while the assumption of a constant $(\gamma - 1)$ can cause deviations by a factor of ~ 2. The stellar flux impinging with this angle into the disk is

$$F^*_{irr} = \alpha\,\frac{L_*}{4\pi R^2}\,. \tag{2}$$

This equation assumes that the entire star is visible from the considered point on the disk surface. If the disk would stretch all the way to the star, the bottom half of the star would not be visible and a correction would have to be made. However, since we consider disks with large inner holes, the transition from the star being invisible to the star being fully visible will be sharp, and we ignore this effect.

The flux F^*_{irr} is absorbed in the upper layers of the disk, which will reradiate half of the flux away from the disk and

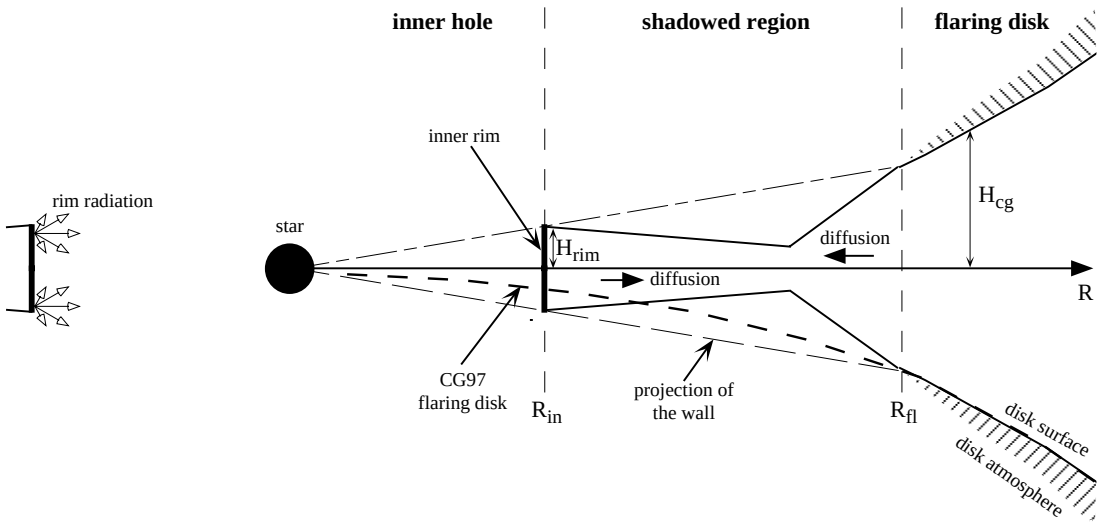

FIG. 1.—Sketch of the geometry of the model

half down into the disk's deeper layers. A fraction ψ_s of this flux will be absorbed by the interior, where ψ_s is a dimensionless number in between 0 and 1 that accounts for the possibility that the disk interior is not fully optically thick to the emission of the surface layer. We assume the disk interior to be isothermal with a temperature T_i, which is a very good approximation for optically thick disks. This interior will emit a flux $F_{\rm emit}$ given by

$$F_{\rm emit} = \psi_i \sigma T_i^4 , \tag{3}$$

where ψ_i accounts for the possibility that the disk interior is not fully optically thick to its own emission. For a fully optically thick disk one has $\psi_s = \psi_i = 1$. The formulas for determining ψ_s and ψ_i for non–optically thick cases are given in Appendix A, § A1.

By equating $\frac{1}{2}\psi_s F^*_{\rm irr} = F_{\rm emit}$, one can solve for T_i and find

$$T_i = \left(\frac{\alpha\psi_s}{2\psi_i}\right)^{1/4}\left(\frac{R_*}{R}\right)^{1/2} T_* . \tag{4}$$

The disk will be almost isothermal in the vertical direction, leading to a Gaussian density distribution with a constant pressure scale height $h_{\rm cg}$ given by

$$\frac{h_{\rm cg}}{R} = \left(\frac{T_i}{T_c}\right)^{1/2}\left(\frac{R}{R_*}\right)^{1/2} , \tag{5}$$

where $T_c = GM_*\mu m_p/kR_*$ is the virial temperature at the stellar surface. The ratio of the disk surface height $H_{\rm cg}$ to the pressure scale height $h_{\rm cg}$ is a dimensionless number $\chi_{\rm cg}$ of order unity:

$$H_{\rm cg} = \chi_{\rm cg} h_{\rm cg} . \tag{6}$$

Usually this $\chi_{\rm cg}$ will lie somewhere in between 2 and 6, but it can be self-consistently determined from the grazing angle α, the surface density Σ, and the Planck mean opacity at the stellar temperature $\kappa_{\rm P}(T_*)$. The way to do this is described in § A2.

2.1.2. *Disk Surface Layer*

Since the disk surface layer is defined as the layer of matter in direct sight of the central star up to grazing optical depth $\tau_\alpha \simeq 1$, the temperature in this layer can be estimated from the optically thin expression

$$T_s = \frac{1}{\epsilon_s^{1/4}}\left(\frac{R_*}{2R}\right)^{1/2} T_* , \tag{7}$$

where ϵ_s is the ratio of the Planck mean opacities at T_s and T_*. Quantities describing the surface layer carry the subscript s. The Planck mean opacity is defined as

$$\kappa_{\rm P}(T) = \frac{\int_0^\infty B_\nu(T)\kappa_\nu\, d\nu}{\int_0^\infty B_\nu(T) d\nu} . \tag{8}$$

The flux from the surface layer in both the upward and the downward direction is

$$\begin{aligned} F_s &= 2\pi\Delta\Sigma\int_0^\infty B_\nu(T_s)\kappa_\nu\, d\nu \\ &= 2\Delta\Sigma\kappa_{\rm P}(T_s)\sigma T_s^4 , \end{aligned} \tag{9}$$

where $\Delta\Sigma$ is the surface density of the layer. Energy conservation implies $F_s = (\psi_i/\psi_s)\sigma T_i^4$, so the surface density of the layer is

$$\Delta\Sigma = \frac{1}{2\kappa_{\rm P}(T_s)}\frac{\psi_i}{\psi_s}\frac{T_i^4}{T_s^4} . \tag{10}$$

In our treatment of the surface layer we ignore scattering. It should be pointed out that, while the effect of this approximation on the structure of the disk is small, the effect on the SED might be nonnegligible.

2.2. *Inner Rim*

We assume in the following that the disk is truncated on the inside by dust evaporation. The disk may continue toward the star in purely gaseous form, but as long as the gas is optically thin to the stellar radiation, we can neglect its effects and describe the disk structure as if it has a true inner hole.

The inner disk radius $R_{\rm rim}$ is determined by requiring that the disk temperature equals the dust evaporation temperature, which we take to be $T_{\rm evap} = 1500$ K. The inner rim of the disk exposes a vertical surface to direct stellar radi-

ation and will therefore be hotter than the flaring disk model at the same radius. For a given inner radius $R_{\rm rim}$ of the disk, the blackbody temperature of the rim is

$$T_{\rm rim} = \left(\frac{L_*}{4\pi R_{\rm rim}^2 \sigma}\right)^{1/4} \left(1 + \frac{H_{\rm rim}}{R_{\rm rim}}\right)^{1/4}, \quad (11)$$

which is derived by equating the emitted blackbody flux $\sigma T_{\rm rim}^4$ to the received flux from direct stellar radiation $L_*/4\pi R_{\rm rim}^2$. The factor $(1 + H_{\rm rim}/R_{\rm rim})^{1/4}$ approximately accounts for the effect of self-irradiation, i.e., irradiation of the rim by its own emission. The ratio $H_{\rm rim}/R_{\rm rim}$ is an approximate expression for the covering fraction of the rim enclosing the cavity $R < R_{\rm rim}$. We assume $R_* \ll R_{\rm rim}$ and therefore neglect that the star itself obscures a small region on the far side of the rim. The vertical height of the inner rim, $H_{\rm rim}$, is given by

$$H_{\rm rim} = \chi_{\rm rim} h_{\rm rim}, \quad (12)$$

where $h_{\rm rim}$ is the pressure scale height at the inner rim

$$h_{\rm rim} = \sqrt{\frac{k T_{\rm rim} R_{\rm rim}^3}{\mu m_p G M_*}} \quad (13)$$

and $\chi_{\rm rim}$ is a dimensionless constant (similar to $\chi_{\rm cg}$ defined above). In § A3 we show how to compute $\chi_{\rm rim}$ self-consistently.

By equating $T_{\rm rim} = T_{\rm evap} \equiv 1500$ K, one can solve for $R_{\rm rim}$ by writing equation (11) as

$$R_{\rm rim} = \left(\frac{L_*}{4\pi T_{\rm rim}^4 \sigma}\right)^{1/2} \left(1 + \frac{H_{\rm rim}}{R_{\rm rim}}\right)^{1/2} \quad (14)$$

and iterate until convergence. If the self-irradiation can be ignored ($H_{\rm rim}/R_{\rm rim} \ll 1$), then no iteration is needed. However, as it turns out, for most HAeBe stars the ratio $H_{\rm rim}/R_{\rm rim}$ (which is the covering fraction of the inner rim) is of the order of 0.1–0.25, and therefore the effects of self-irradiation cannot be ignored.

Self-irradiation has the effect of pushing out the inner radius, if the temperature of the inner rim is fixed at 1500 K. This means that the blackbody-emitting surface is larger. But since only part of this radiation will escape to infinity (the other part being again absorbed by the inner rim itself), energy remains conserved. Once $R_{\rm rim}$ is determined, the vertical height of the inner rim $H_{\rm rim}$ automatically follows from equations (12) and (13), and one has the basic properties of the inner rim fixed.

2.3. *Shadowed Region*

The inner rim will always be significantly higher than the flaring disk height because it is hotter by a factor of at least $(2/\alpha)^{1/4}$. In general this will roughly yield a puffing-up ratio of $H_{\rm rim}/H_{\rm cg} \simeq 2$. The disk material immediately behind this inner rim will therefore be deprived of direct stellar light, since the rim casts a shadow over the disk behind it. This region of the disk is cooler than predicted by CG97 models and therefore is not flared. Only at much larger distance, where the disk comes out of the inner rim shadow and is illuminated again by the stellar light, may flaring occur. Since the shadow covers every point (R, z) for which $z/R < H_{\rm rim}/R_{\rm rim}$, the radius $R_{\rm fl}$ at which the disk can again be described by the CG97 model is computed by solving the following equation:

$$H_{\rm rim}(R_{\rm rim}) \frac{R_{\rm fl}}{R_{\rm rim}} = H_{\rm cg}(R_{\rm fl}). \quad (15)$$

For $R < R_{\rm fl}$, the most important sources of irradiation are the NIR emission of the rim itself and the fraction of stellar light that is scattered toward the disk by the edge of the rim, or by a halo of dust surrounding the star-plus-disk system (Natta 1993). In addition to this, radiative diffusion can exchange energy between neighboring annuli. However, rough estimates of these effects show that the radiation emitted by this shadowed region of the disk is negligible compared to the emission of the rim and of the outer disk, directly heated by the star.

However, the disk structure immediately behind the inner rim is of importance for our discussion because we need it in order to estimate the quantity $\chi_{\rm rim}$ in equation (12), i.e., the ratio of the photospheric to the pressure scale height at $R_{\rm rim}$ (see § A3). At this location of the disk none of the irradiation sources play any significant role. Instead, direct radiative diffusion from the inner rim will dominate the energy balance there (see Fig. 2).

It is difficult to determine exactly what the structure of the disk is in this diffusive region, but a simple model for this is provided below.

The inner rim of the diffusive region receives direct starlight. This radiation is absorbed and reemitted by the dust grains. Some of this radiation will once again be absorbed and reemitted. In the end, most radiation will, after one or more absorption/reemission events, escape from the hot inner rim surface. However, a small fraction of the radiation remains trapped within the disk and diffuses toward larger radii. The diffusive flux is proportional to the gradient of the temperature of the disk's interior. Since it is expected that the temperature has a net decrease outward, there will be an outward-pointing diffusive flux. As a package of energy has moved one surface height H toward larger radii, it has had an equal chance of having escaped from the disk's surface. This is true for each surface height it travels outward. The differential equation for the disk's temperature would be approximately

$$\frac{d(RT^4)}{dR} \simeq -\frac{RT^4}{H}, \quad (16)$$

where T is a rough estimate of the temperature of the disk interior at radius R. In this equation we have included the

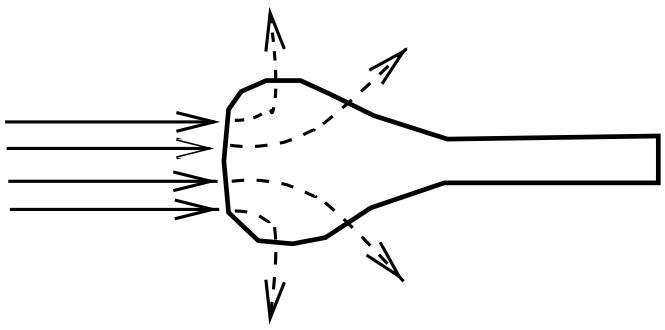

FIG. 2.—Sketch of the two-dimensional radiative diffusion process through the disk inner edge. The solid arrows indicate direct radiation from the star. The dashed arrows represent the diffusion through the disk.

effect of geometric dilution due to the cylindrical geometry, hence the factor R inside the brackets of the differentiation. A similar factor H is not included, since H is expected to decrease outward, which would lead to an unphysical geometrical compression of the radiation field. In this diffusive region the disk could be vertically nonisothermal, but we ignore this effect in this simple treatment. In addition, we ignore the fact that the definition of H, as given in § 2.1, is not very meaningful in this nonirradiated region. Now, since $H \propto (TR^3)^{1/2}$ (see, e.g., eq. [5] and assume for convenience that $\chi =$ constant), the temperature T can be eliminated from the differential equation, leaving an ordinary differential equation to be solved for H:

$$\frac{d \log (H^8 R^{-11})}{dR} = -\frac{1}{H} . \tag{17}$$

This equation can be solved numerically.

For $H \ll R$, it reduces to

$$\frac{d(H/R)}{dR} = -\frac{1}{8R} , \tag{18}$$

which shows that at the inner edge H/R approximately goes as $H/R = H(R_{\rm rim})/R_{\rm rim} - \log (R/R_{\rm rim})/8$.

In this approximation the disk has lost all its energy at $R - R_{\rm rim} = 8H(R_{\rm rim})$ and has collapsed to zero height. This would of course be unphysical, and before this happens, other heating mechanisms will have taken over, such as the ring emission mentioned above, light scattering off a spherical halo surrounding the disk-plus-star system, interstellar radiation, or viscous dissipation.

Equation (17), but with an opposite sign, describes the diffusion of energy inward from the still flaring part of the disk into the shadowed region.

2.4. *Self-Irradiation Corrections to Flaring Part*

For $R > R_{\rm fl}$ the flaring disk is in full view of the central star, and the irradiation is clearly dominated by the stellar flux. However, for HAeBe stars the luminosity of the inner rim can be of order 20% of the stellar flux. Moreover, the emission of the inner rim is not isotropic. In close to polar directions, the projected surface of the rim is small in the flux correspondingly low. For a point on the surface of the flaring disk, on the other hand, the projected surface of the rim is close to $4R_{\rm rim}H_{\rm rim}$ (see Appendix B). Therefore, the relative flux contribution of the rim at the disk surface will be even larger than the angular average of 20%. For an accurate determination of the disk structure in the flared region one should include this secondary irradiation. We consider the inner rim as a cylinder. The irradiative flux is then (see Appendix B)

$$F_{\rm irr} = \alpha(R) F_* + \frac{2}{\pi} \alpha(R) \sigma T_{\rm rim}^4 \left(\frac{R_{\rm rim}}{R}\right)^2 \times \cos \theta (\delta \sqrt{1-\delta} + \arcsin \delta) . \tag{19}$$

This irradiative flux $F_*^{\rm irr}$ is then equated to the disk's reemission flux $F_{\rm emit}$ (eq. [3]), thus yielding the corrected value of T_i.

For the surface layer temperature one also has to add the two sources of irradiation, but in order to compute the ϵ_s factor in equation (7), one now has to replace the $\kappa_{\rm P}(T_*)$ in the definition of ϵ_s (§ 2.1.2) with

$$\kappa_{\rm irr} \equiv \frac{\int_0^\infty \kappa_\nu F_\nu^{\rm irr} d\nu}{\int_0^\infty F_\nu^{\rm irr} d\nu} . \tag{20}$$

3. COMPUTING THE SED

Once the disk structure is known, one can compute the emerging spectrum. In principle, one requires a two-dimensional (axially symmetric) ray-tracing program to compute the SED at various inclination angles. This is because the disk structure, in particular for HAeBe stars, is far from being flat, and self-occultation is a real possibility (Chiang & Goldreich 1999). However, in this section we shall use a simplified treatment of inclination, therefore limiting ourselves to inclinations that are not too edge-on.

3.1. *Spectrum of Flaring Disk*

The determination of the spectral components from the flaring part of the disk is relatively straightforward and has been described fully by CG97. We confine ourselves here to a quick reference of the equations. The emission from the interior of the disk is

$$F_\nu^i(d, i) = 2\pi \cos i \int_{R_{\rm fl}}^{R_{\rm out}} \left\{1 - \exp\left[\frac{-\Sigma(R)\kappa_\nu}{\cos i}\right]\right\} \times B_\nu[T_i(R)] \frac{R}{d^2} dR , \tag{21}$$

where d is the distance from the observer to the source and i the inclination angle ($i = 0$ means face-on). This equation remains valid at wavelengths where the disk interior becomes optically thin. The emission from the surface layer is

$$F_\nu^s(d, i) = 2\pi \int_{R_{\rm fl}}^{R_{\rm out}} \left\{1 + \exp\left[\frac{-\Sigma(R)\kappa_\nu}{\cos i}\right]\right\} \times B_\nu[T_s(R)] \Delta\Sigma\kappa_\nu \frac{R}{d^2} dR , \tag{22}$$

where $\Delta\Sigma$ is given by equation (10). Equation (22) includes the effect of also seeing the surface layer on the other side of the disk at wavelengths where the disk is optically thin.

3.2. *Spectrum of Inner Rim*

The inner rim is assumed to be a cylinder emitting on its inner side as a blackbody with temperature $T_{\rm rim}$. To compute the emission from this rim, we have to include inclination effects. Clearly, if $i = 0$ (face-on), then the emission from the rim is zero (although in reality the rim may be more rounded off and therefore also visible at face-on inclination). For $i = \pi/2$ (edge-on) the emission is also zero because the rim is self-occulting. The projected surface, as seen by an observer at inclination i, is given by equation (B2). For not too large inclination angles we are in the regime $\delta \ll 1$, and one can then write

$$F_\nu^{\rm rim}(d, i) = 4 \frac{R_{\rm rim} H_{\rm rim}}{d^2} (\sin i) B_\nu(T_{\rm rim}) . \tag{23}$$

The total luminosity of the rim equals $L_{\rm rim} = \Omega_{\rm rim} L_*$, where $\Omega_{\rm rim} = H_{\rm rim}/R_{\rm rim}$ is the covering factor of the rim (i.e.,

the fraction of the sky covered by the rim as seen from the perspective of the star). For large $H_{\rm rim}/R_{\rm rim}$ this will therefore give a strong contribution to the SED.

4. RESULTS

In this section we show the structure of the computed models and the SEDs produced by models with different parameters.

4.1. *Example Model*

To illustrate the general features of our model, we set up an example model consisting of a star with $T_{\rm eff} = 9500$ K, $L_* = 47\ L_\odot$, and $M_* = 2.4\ M_\odot$ (we take the stellar spectrum to be a blackbody for simplicity) and a disk with outer radius $R_{\rm out} = 400$ AU and inner radius at the dust condensation point ($T_{\rm rim} = 1500$ K), which for this setup is at $R_{\rm rim} = 0.47$ AU. The disk's surface density goes as $\Sigma(R) = 2 \times 10^3 (R/{\rm AU})^\beta$, with $\beta = -1.5$, and we assume a gas-to-dust ratio of 100. The disk is seen at an inclination angle $i = 45°$. We take a simple model for our dust opacity: a mixture of amorphous carbon and astronomical silicate in a ratio 0.05. The amorphous carbon opacity is computed according to the simple recipe given by Ivezic et al. (1997), while the silicate opacity is that of Draine & Lee (1984). We ignore scattering. The SED depends on dust properties in various ways, and variations of the opacity from object to object and between grains in the disk surface layer and midplane are known to occur (e.g., Bouwman et al. 2000). However, this aspect of the problem is outside the scope of this paper and is not relevant to the conclusions we reach.

Figure 3 shows the structure of the disk for these stellar parameters. The inner edge is at $R = 0.52$ AU, beyond which the vertical height of the inner edge quickly declines (although when plotted linearly in R this decline is not so rapid as it seems in this figure). For $R > 6.6$ AU the disk has the usual flaring shape, but with self-irradiation effects added. The region between $0.52 < R < 6.6$ AU is the shadowed region. Between $0.52 < R < 1$ AU the disk is dominated by radiative diffusion from the inner edge outward, as described in § 2.3. In the region $1 < R < 1.5$ AU radiative diffusion from outside inward dominates. For radii $1.5 < R < 6.6$ AU the disk is still not in sight of the star itself, but it receives flux from the inner rim, which is sufficiently strong to keep up the disk. Inward radiative diffusion prevents a sudden jump to the fully flared region starting at $R > 6.6$ AU, although the surface temperatures cannot be prevented from jumping. The inward radiative diffusion is estimated using an equation similar to equation (16), but with opposite sign. The details of the structure between $1 < R < 6.6$ AU are not very important, since this region hardly contributes to the SED. For this reason we are content with the rather crude description presented here.

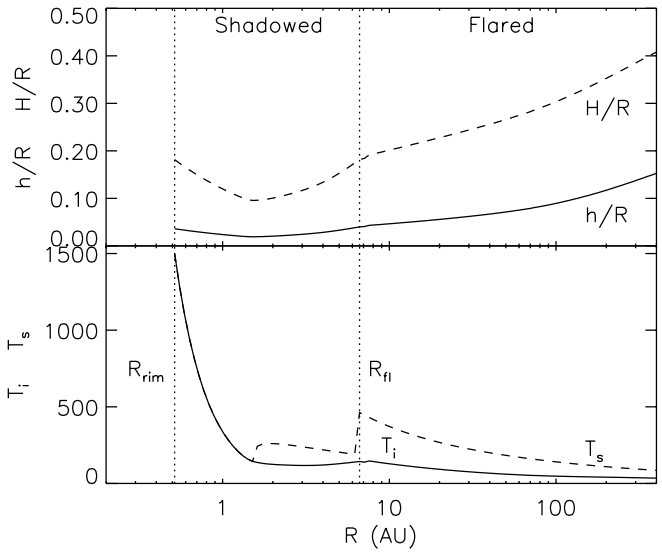

FIG. 3.—Structure of example model E3. *Top:* Disk pressure scale height (*solid line*) and surface height (*dashed line*), both divided by radius. *Bottom:* Midplane temperature (*solid line*) and temperature of the surface layer (*dashed line*).

Figure 4 shows the resulting SED for the example model. We show for reference in panel (*a*) the SED predicted by a CG97 model, where the effects of the inner radius (emission and shadow) are ignored. Panel (*b*) shows the effect of including the emission from the inner rim, assumed to have the height of the flaring disk at that radius. In this case, the SED in the mid- to far-IR remains unmodified, but a new component appears in the NIR. Finally, panel (*c*) shows the results of the self-consistent calculation described in the previous sections. One can see that the NIR emission from the puffed-up rim increases, but the inner rim starts to cast a shadow over the disk, thereby suppressing some of the mid- and far-IR emission. Panel (*d*) shows a blowup of the 1–100 μm region, where the different effects of the inner rim can be clearly seen.

In the following subsections we show how the model-predicted SEDs change as a function of some of the model parameters. We summarize some of the characteristics of the models and of the SED properties in Table 1.

4.2. *Effect of Inclination Angle*

In Figure 5*a* we show how the SED of our example model changes with the inclination with respect to the line of sight. We consider here only values of i such that the line of sight does not intercept the outer disk.

One sees that for nearly face-on inclinations the NIR excess is less prominent and the far-IR is strong, while for nearly edge-on inclinations the opposite is true. By varying i from 50° to 20°, the ratio $F_{\rm NIR}/F_*$ decreases from 0.18 to 0.08, while the IR excess at wavelengths longer than 7 μm increases from 0.32 to 0.35. This is because the disk radiates predominantly toward the poles, while the inner rim radiates predominantly toward the equator. The emission features are optically thin features and are therefore less affected by the inclination. Only when the inclination would exceed the opening angle of the flared disk would these features go from emission into absorption because of the obscuration effect of the disk itself. However, in order to model this properly, we would need a multidimensional ray-tracing computation, which is beyond the scope of this paper.

4.3. *Effect of Varying Inner Radius*

The inner rim in our models is located at the dust evaporation radius and is therefore fixed once the stellar parameters are defined. Nevertheless, it is instructive to see the effects of varying the inner radius on the SED because it helps in clarifying the properties of our models, and we plot in Figure 5*b* the SED of our standard model for varying

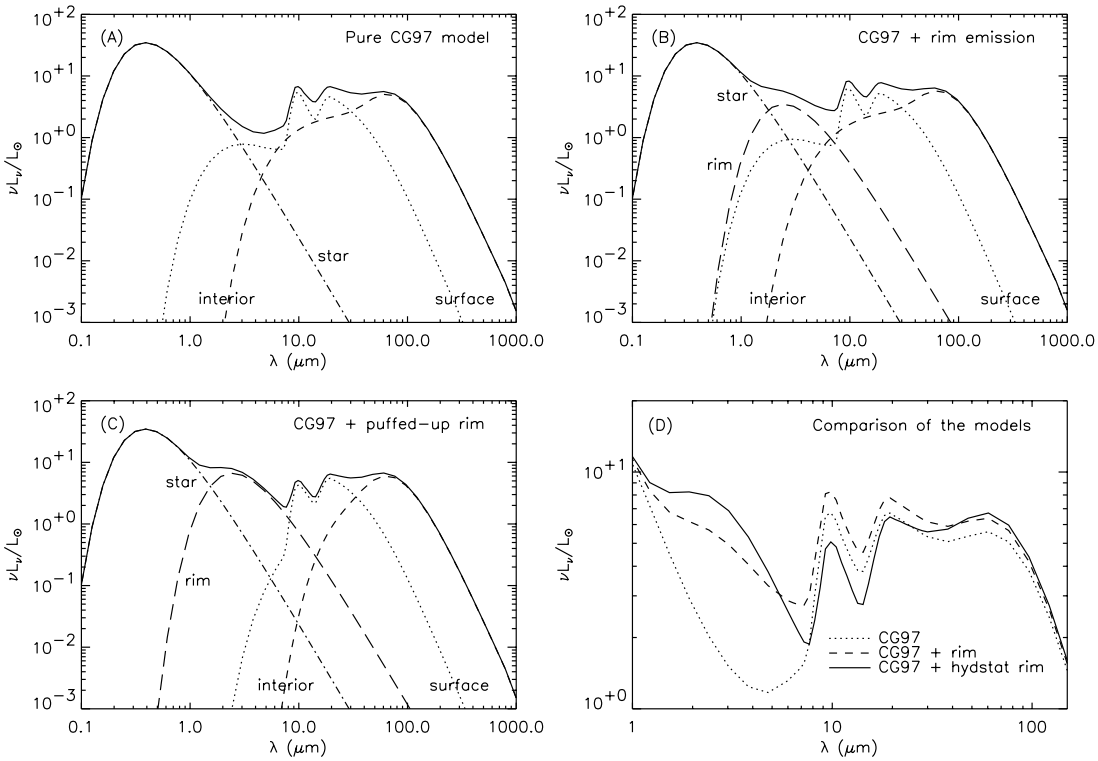

FIG. 4.—SED of the example model (see § 4.1), computed according to (*a*) the unmodified CG97 model (model code E1), (*b*) the CG97 model with inclusion of the emission from the inner rim (model code E2), and (c) with a self-consistent puffed-up inner rim (model code E3). In panel (*d*) the three SEDs are compared. In the unmodified CG97 model, the SED (*solid line*) is the sum of the emission of the star (*dot-dashed line*), the disk interior (*dashed line*), and the disk surface (*dotted line*). When the emission from the inner edge is added, without modifying the vertical height of the inner rim, a blackbody component at NIR wavelengths is added to the SED (*long-dashed line* in panel [*b*]). When the height of the inner rim is consistently computed, the SED is also the sum of four components (same symbols as in panel [*b*]), but the NIR emission increases, and a shadow is cast over the disk, thus suppressing some of the disk emission.

TABLE 1

PROPERTIES OF DIFFERENT MODELS DISCUSSED IN THIS PAPER

Series	Figure	Model	$T_{\rm eff}$	$F_*/F_\odot$	Σ_0/g cm^{-2}	β	$R_{\rm rim}$/AU	$R_{\rm fl}$/AU	$H_{\rm rim}/R_{\rm rim}$	$\chi_{\rm rim}$	$F_{\rm NIR}/F_*$	$F_{\rm IR}/F_*$	$F_{\rm NIR}/F_{\rm IR}$	$F_{10}/F_{7.7}$
Example	4	E1	9500	47	2000	−1.5	0.47	0.0	0.11	5.3	0.03	0.35	0.08	4.7
		E2	9500	47	2000	−1.5	0.50	0.0	0.10	2.9	0.12	0.50	0.24	3.6
		E3	9500	47	2000	−1.5	0.52	6.6	0.18	5.0	0.17	0.50	0.33	3.5
Inclination.....	5*a*	I1 (50°)	9500	47	2000	−1.5	0.52	6.0	0.18	5.0	0.18	0.50	0.36	3.2
		I2 (35°)	9500	47	2000	−1.5	0.52	6.0	0.18	5.0	0.13	0.47	0.28	3.9
		I3 (20°)	9500	47	2000	−1.5	0.52	6.0	0.18	5.0	0.08	0.43	0.19	5.2
$R_{\rm rim}$	5*b*	R1	9500	47	2000	−1.5	0.20	2.2	0.15	5.3	0.10	0.48	0.21	6.6
		R2	9500	47	2000	−1.5	0.40	3.5	0.17	5.1	0.15	0.50	0.30	4.4
		R3	9500	47	2000	−1.5	0.80	7.9	0.20	4.9	0.18	0.50	0.36	2.3
$H_{\rm rim}$	5*c*	H1	9500	47	2000	−1.5	0.52	6.0	0.18	5.0	0.16	0.49	0.34	3.4
		H2	9500	47	2000	−1.5	0.52	17.0	0.22	6.0	0.20	0.48	0.43	1.9
		H3	9500	47	2000	−1.5	0.53	35.0	0.26	7.0	0.25	0.49	0.50	1.2
		H4	9500	47	2000	−1.5	0.54	70.0	0.30	8.0	0.29	0.48	0.60	0.8
Σ power	5*d*	S1	9500	47	5	−0.5	0.50	2.9	0.12	3.5	0.11	0.48	0.23	4.8
		S2	9500	47	100	−1.0	0.52	4.2	0.16	4.3	0.14	0.48	0.29	3.9
		S3	9500	47	2000	−1.5	0.52	6.0	0.18	5.0	0.16	0.49	0.34	3.4
		S4	9500	47	4×10^4	−2.0	0.52	6.0	0.20	5.6	0.19	0.51	0.37	3.2
ZAMS	6	Z1 (B2)	22000	1000	2000	−1.5	5.88	68.0	0.27	4.5	0.31	0.51	0.60	2.6
		Z2 (A0)	8900	50	2000	−1.5	0.53	6.1	0.18	5.0	0.16	0.48	0.34	3.4
		Z3 (G2)	5900	1	2000	−1.5	0.08	0.73	0.12	5.4	0.10	0.48	0.21	3.3
		Z4 (M2)	3500	0.05	2000	−1.5	0.015	0.22	0.09	5.7	0.07	0.48	0.15	2.2
T Tauri	7	T1	3800	0.76	2000	−1.5	0.064	0.64	0.14	5.4	0.13	0.60	0.21	3.0
AB Aur	8	A1	9520	48.3	10^4	−2.0	0.52	8.1	0.19	5.4	0.22	0.45	0.49	2.5

NOTE.—The first three columns are for model identification, the next seven list model parameters and disk properties, and the last four columns list computed observables evaluated from the star-subtracted SED, where $F_{\rm NIR}$ is the flux in the interval 1.25–7 μm, $F_{\rm IR}$ the flux at $\lambda > 1.25$ μm, and F_{10} and $F_{7.7}$ the fluxes at 10 and 7.7 μm, respectively. F_* is the integrated stellar flux.

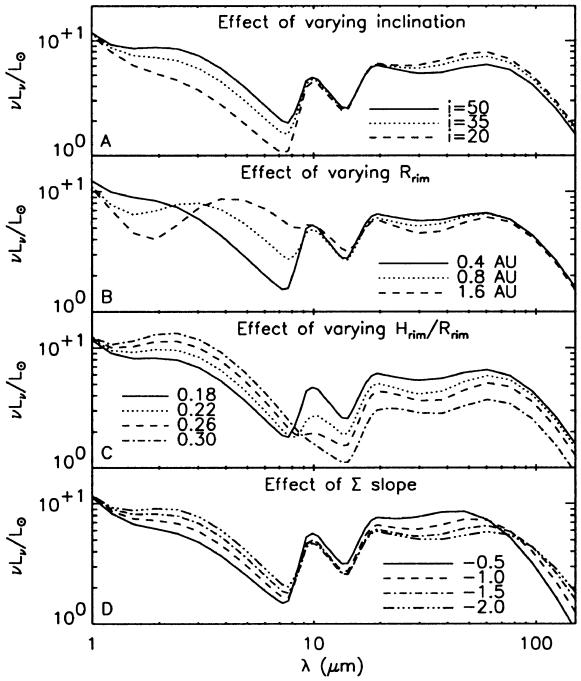

FIG. 5.—Observed SED of our example model, for varying input parameters. For all figures the inclination angle is $i = 45°$, except for the one that shows the effect of varying inclination.

R_{rim}. The effect is strong in the NIR, where both the excess luminosity and its shape change drastically. For larger R_{rim}, the NIR "bump" is enhanced, with a peak that moves toward longer wavelengths, but the flux around 1 μm decreases as the temperature of the inner rim decreases.

There are also, barely visible in the figure, some changes at intermediate wavelengths due to the reduction of shadowing, which increases the contribution of the disk surface layer also around 50 μm.

4.4. *Effect of Shadow on the 10 μm Feature*

If the height of the puffed-up inner rim is computed according to the equation for vertical pressure balance (eq. [5] with T_i replaced by T_{rim}), then the shadow that the rim projects over the disk will usually extend up to a radius of roughly 10–20 times the inner radius. This ratio turns out to be fairly robust in our model, which can be attributed to the fact that the ratio of T_{rim}/T_{cg} is fairly constant for all model parameters. At 10–20 times R_{rim} the surface layer temperature is about 4.5–6.3 times lower than T_{rim} (which is 1500 K by definition in our model). This means that the shadow starts to affect the regions of the disk's surface layer that emit the 10 μm feature, which lies at 5 times longer wavelengths than the NIR bump. This effect is already visible when comparing our standard model to the result of a CG97 model (Figs. 4*c* and 4*d*).

If, for some reason, we have underestimated the height of the inner rim (which is the most difficult quantity to determine in our models), this might have repercussions on the predicted 10 μm flux. To investigate this effect, we have artificially enhanced the height of the puffed-up inner rim (i.e., we have relaxed the assumption that the disk is here in vertical pressure balance) and computed the SED. The results are shown in Figure 5*c*, where we have increased χ_{rim} to values as large as 8. For increasing inner rim height, the 2 μm bump is of course enhanced, but the major effect on the SED is the change at longer wavelengths due to the fact that the shadow extends to larger radii, eventually to most of the disk. The 10 μm feature is the first part of the SED to be affected by the increase of χ_{rim} and has entirely disappeared for $\chi_{rim} = 8$. The 20 μm silicate feature is less affected because it is emitted at lower temperature and hence at larger radius. The total IR flux is conserved: the increase in NIR flux goes at the cost of the mid-IR and far-IR flux (see Table 1, models H1–H4).

The exact value of χ_{rim} depends on a number of properties that are difficult to constrain, such as the shape of the disk behind the rim and the dust properties. However, its exact value is not crucial for the discussion of the basic idea behind our model, which revolves around two issues: the presence of a puffed-up inner rim at roughly the dust evaporation radius, naturally producing the NIR bump, and a proper consideration of energy conservation, which implies that we must take into account the shadow that the rim projects onto the disk. The exact shape of the rim is, in a way, a secondary aspect.

4.5. *Effect of Σ-Slope*

The surface density $\Sigma(R)$ is an unknown quantity and serves as an input to the model. The results of the models turn out not to be very dependent on the surface density. The main effect it can have is changing the balance between NIR and far-IR radiation and the slope of the SED at far-IR/submillimeter wavelengths. To demonstrate this, we show models with $\Sigma = \Sigma_0(R/R_0)^\beta$ for different values of β. For each of these models we tune the Σ_0 such that the total covering fraction of the disk $\Omega = H(R_{out})/R_{out}$ is equal to $\Omega = 0.4$ (see Table 1 for the resulting values of Σ_0). The rest of the parameters are the same as for the example model. The results are shown in Figure 5*d*.

4.6. *Behavior of the Model for Varying Stellar Type*

The behavior of the NIR excess as a function of the stellar type of the central star is shown in Figure 6, which plots the SEDs of four stars along the zero-age main sequence (ZAMS) ranging from spectral type B2 to M2 (see Table 1). The NIR bump is clearly visible in stars of spectral type A and earlier but tends to disappear in later stars. This is due to two effects. First of all, for cooler central stars the stellar flux peaks at longer wavelength and therefore swamps the

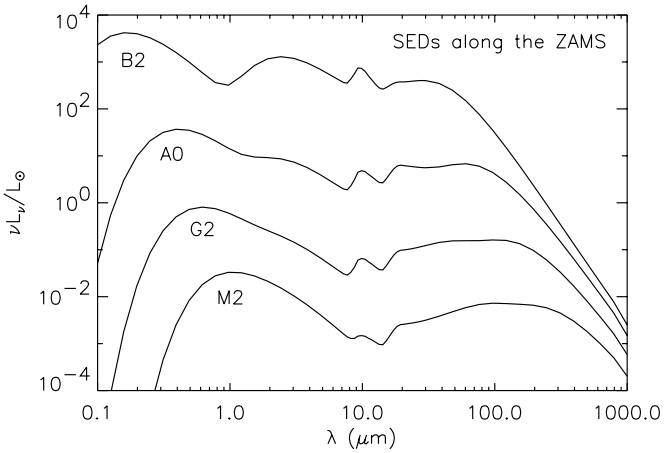

FIG. 6.—Model-predicted SED for ZAMS stars of different spectral type. The stellar parameters are given in Table 1.

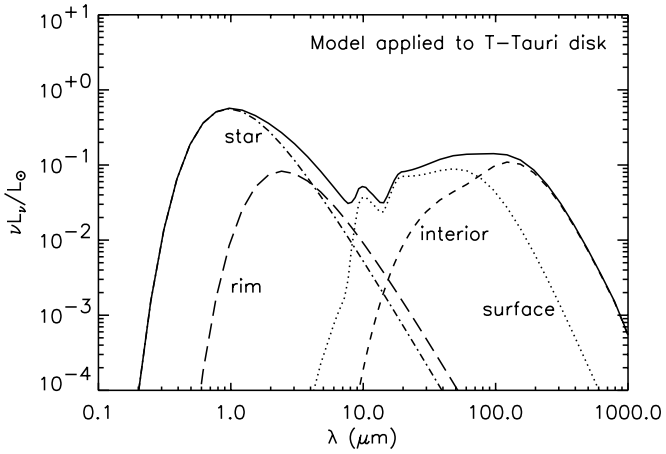

FIG. 7.—SED of a TTS of $T_{\rm eff} = 3800$ K, $L/L_\odot = 0.76$, and $M/M_\odot = 0.55$. The various line styles represent the different components contributing to the SED in the same way as in Fig. 4.

NIR emission of the disk. In addition to this, the ratio of the covering factor of the puffed-up inner rim (in vertical hydrostatic equilibrium) to the covering fraction of the flaring part of the disk decreases for later spectral types. These factors determine the relative importance of the various components of the SED, as can be seen from Table 1. As we consider stars of later spectral types, the NIR excess luminosity decreases by a factor of 2. The various components that contribute to the observed SED of a typical TTS are shown in Figure 7.

Our disk models provide a natural explanation for the fact that the NIR "bump" is observed in HAeBe stars, while it is not noticeable in stars of later spectral type, and in particular in TTSs. We return to this point in the following section.

5. DISCUSSION

5.1. *Disk Physics*

It is currently not clear whether a sharp inner rim can be stable in the way described here. The thermal pressure that is responsible for the rim height will act not only in the vertical but also radially toward the star. We can think of two possibilities to stabilize the rim. The space between the star and the disk could be filled with optically thin gas, and the gas pressure could stabilize the rim. A second possibility would be centrifugal force. If the inner rim rotates at slightly super-Keplerian speeds, it could counter the gas pressure. This super-Keplerian rotation might be automatically created if material flowing inward because of an initial pressure gradient preserves its angular momentum. A dynamical study of the problems would be very interesting but is beyond the scope of the current study.

Radiation pressure on dust grains may also affect the structure of the inner rim. In the upper regions, the gas drag may not be strong enough to keep small dust grains from being blown away by radiation pressure, an effect that would locally decrease the dust-to-gas ratio and therefore opacity and the rim height. On the other hand, radiation pressure could also lead to gas-dust separation at the inner rim if some low-level accretion is still going on in the disk. The star would then accrete only the gas while the dust would stay in the rim and accumulate with time. This might cause an increase of the rim height, compensating for the removal of grains by radiation pressure. Radiation pressure on dust grains can also have effects in the flaring part of the disk, by pressing the grains deeper into the disk and reducing the surface height there. All these processes are poorly studied and deserve more attention in future work.

Another point of concern is the question whether the flaring part of the disk is dynamically stable. If one takes the disk equations of CG97, and those described in the present paper, at face value, one can show that the disk is unstable to self-shadowing effects caused by a perturbation in the vertical scale height (Dullemond 2000; Chiang 2000). In fact, the shadowed region outside the inner rim is an example of this shadowing effect. This instability acts on a Keplerian timescale and could cause the entire flaring disk to collapse into the shadow of the inner rim. A recent study, however, shows that multidimensional radiative transfer effects can stabilize the disk for certain disk parameters (C. P. Dullemond 2001, in preparation), and the inclusion of self-consistent vertical structure of the disk models may enhance this stabilizing effect.

5.2. *Comparison with the Observations*

Disk models where the irradiation from the star dominates the heating provide a good fit to most properties of pre–main-sequence stars over a large range of masses (see, e.g., D'Alessio et al. 1998, 1999; CG97; Chiang et al. 2001). However, there are a few points that have remained unclear, and we think that the better treatment of the inner disk with respect to previous models provides an answer to one of them, namely, the long-standing puzzle of the NIR bump in the SEDs of HAeBe stars.

In Figure 8 we show a fit of our model to the SED of AB Aurigae, one of the best studied HAe stars. The basic features of the SED are well reproduced by the model: the 3 μm bump, the 10 μm feature, the far-IR plateau, and the sharp decline toward millimeter wavelengths. Our model has only a few free parameters [i, $\Sigma(R)$, $R_{\rm out}$, and the dust opacity table], so the fact that the data can be fitted in a reasonable way gives support to our model. The inclination angle of $i = 65°$ needed for this fit is larger than what most observations suggest (e.g., Natta et al. 2001 and references therein). However, the assumption of a perfectly vertical rim

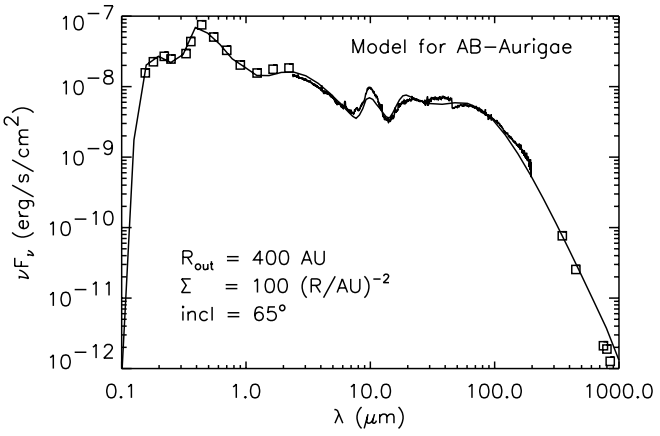

FIG. 8.—Best fit to AB Aur. Parameters are $M_* = 2.4\ M_\odot$, $L_* = 47\ L_\odot$, $T_* = 9520$ K, $\Sigma = 10^4 (R/{\rm AU})^{-2}$, $R_{\rm out} = 400$ AU, $i = 65°$, and $D = 144$ pc. The plot shows the model fit (*solid line*), together with photometry points (*squares*) and the *ISO* SWS and LWS spectra between 2.3 and 200 μm (data from Meeus et al. 2001).

that is responsible for this value may be too simple. A more rounded surface of the inner rim will allow more of the rim radiation to be emitted into polar directions.

Nevertheless, the model-predicted values of $F_{\rm NIR}/F_*$ for A stars (hovering around 0.17) agree well with those observed in four HAe stars by Natta et al. (2001), which range between 0.12 and 0.25, respectively, and by Meeus et al. (2001) in a sample of 14 HAe stars, where $F_{\rm NIR}/F_*$ varies between 0.06 and 0.3 for the group I sources.

Observations show that the "bump" is a more or less constant feature from star to star (Hillenbrand et al. 1992), in contrast to the long-wavelength emission, which is affected by a variety of disk and dust parameters (Meeus et al. 2001). This robustness is naturally reproduced in our model, since to first order the properties of the NIR bump are determined only by the dust sublimation temperature and the covering fraction of the rim, the latter varying only weakly as a function of stellar type.

In spite of this, the "bump" disappears in stars of spectral type F or lower (see Fig. 6). As discussed in § 4.6 and shown in Table 1, this can be explained as being due to two concurring effects. The first is the lower covering angle of the rim in stars of later spectral type, where dust sublimation occurs closer to the star. The second is the fact that the stellar radiation peaks at longer wavelengths, swamping the rim emission. Thus, even if the shape of the "bump" is the same, it becomes very difficult to see it and to separate the rim contribution from the stellar emission. It is, however, possible that one is seeing the rim emission in some TTS with NIR colors that can only be understood if the disk has an inner radius of a few stellar radii, coinciding with the dust sublimation radius for systems of typical TTS luminosity (Beckwith et al. 1990; Kenyon et al. 1996).

Another interesting aspect of these models is the effect of the shadow that the rim projects onto the disk. The 10 μm silicate emission in our example model has $F_{10}/F_{7.7} = 3.5$, in reasonable agreement with what was observed in HAe stars by Natta et al. (2001). These numbers, however, are very dependent on the properties of the grains in the disk surface layer. A weak or absent 10 μm feature, for example, can be attributed to a dominance of large silicate grains in the disk surface layer (Meeus et al. 2001), to a very high ratio of the visual opacity to the opacity in the feature (Natta et al. 2001), or to an almost perfect cancellation of absorption and emission in disks seen edge-on (Chiang & Goldreich 1999). We propose here still another possibility, namely, that the inner rim in some object is higher than normal because, for example, the rim is not in hydrostatic equilibrium, is thicker in the radial direction, or has a higher $\chi_{\rm rim}$, the ratio of the photospheric to the pressure scale height. As shown in Figure 5*c* and Table 1, a factor of 1.7 increase of $\chi_{\rm rim}$ would be sufficient to suppress the silicate feature entirely.

One point we want to stress here is that a rim structure such as we have described can only exist if the gaseous disk is optically thin to the stellar radiation and the dusty disk is optically thick. If an optically thick gaseous disk extends toward the star closer than the dust evaporation radius, then there is no puffed-up rim and the standard models, which describe the emission of an optically thick disk surface, apply. The formation of a puffed-up rim seems possible only if the accretion rate through the disk is very low, as briefly discussed by Natta et al. (2001). There are indications that this is indeed the case in the majority of HAe stars. Tambovtseva et al. (2001) find accretion rates below $10^{-8}\ M_\odot\ {\rm yr}^{-1}$ from their study of Balmer emission lines in UX Ori (see also Ghandour et al. 1994). There are no similar studies for the hotter HBe stars, and it is clear that in many TTSs accretion rates are high enough to ensure that the inner gaseous disk will be optically thick (Gullbring et al. 1998). This is an additional explanation of why the NIR "bump" is seen only in a minor fraction of TTSs, if at all.

The idea that the emission in the NIR is dominated by the emission of the inner rim finds support in the recent interferometric observations of Millan-Gabet, Shloerb, & Traub (2001). They find that in J and K the emission of AB Aur is best fitted by the emission of a thin shell of radius $\sim$0.3 AU, almost spherical on the plane of the sky. For the luminosity of AB Aur, the inner rim is located at 0.5 AU for dust evaporation temperature around 1500 K. For the low inclination derived from millimeter and optical data ($i \lesssim 45°$; see Natta et al. 2001 and references therein), the rim projected on the plane of the sky is almost spherical. We expect that other HAe stars will be resolved by current and future interferometers, so that the main feature of our models, namely, the fact that the NIR emission comes from a narrow rim located at the dust evaporation radius, will be directly checked.

We would like to thank the anonymous referee for a careful review of the paper. C. D. acknowledges financial support from NWO Pioneer grant 6000-78-333. C. P. D. and C. D. acknowledge support from the European Commission under TMR grant ERBFMRX-CT98-0195 ("Accretion onto Black Holes, Compact Objects, and Protostars"). We thank Rens Waters, Jeroen Bouwman, Caroline Terquem, Claude Bertout, Alex de Koter, Vincent Icke, and Rohied Mokiem for interesting discussions and Gwendolyn Meeus for access to her observational data of HAeBe stars.

APPENDIX A

FINE-TUNING FUNCTIONS

A1. THE ψ PARAMETERS

When the interior of the disk is not optically thick anymore to its own radiation and/or the radiation from the surface layer, then ψ will deviate from unity. For an optically thick interior, the total emitted flux (on a single side) is simply $F_{\rm emit} = \sigma T_i^4$. For non–optically thick cases this becomes

$$F_{\rm emit} = \int_0^\infty \pi B_\nu(T_i)[1 - \exp(-\Sigma\kappa_\nu)]d\nu = \psi_i \sigma T_i^4 , \quad \text{(A1)}$$

with

$$\psi_i = \frac{\int_0^\infty B_\nu(T_i)[1 - \exp(-\Sigma\kappa_\nu)]d\nu}{\int_0^\infty B_\nu(T_i)d\nu} . \tag{A2}$$

The limits for high and low optical depth are

$$\psi_i = \begin{cases} 1 & \text{for } \Sigma\kappa_{\rm P}(T_i) \gg 1 , \\ \Sigma\kappa_{\rm P}(T_i) & \text{for } \Sigma\kappa_{\rm P}(T_i) \ll 1 . \end{cases} \tag{A3}$$

The absorbed flux from the surface layer equals the flux emitted downward by the surface layer multiplied by the absorption fraction $[1 - \exp(-\Sigma\kappa_\nu)]$ and integrated over frequency:

$$F_{\rm abs} = \int_0^\infty 2\pi\Delta\Sigma\kappa_\nu B_\nu(T_s)[1 - \exp(-\Sigma\kappa_\nu)]d\nu = \psi_s F_s , \tag{A4}$$

where F_s is the total flux from the surface layer downward and

$$\psi_s = \frac{\int_0^\infty B_\nu(T_s)\kappa_\nu[1 - \exp(-\Sigma\kappa_\nu)]d\nu}{\int_0^\infty B_\nu(T_s)\kappa_\nu d\nu} . \tag{A5}$$

The limits for high and low optical depth are

$$\psi_s = \begin{cases} 1 & \text{for } \Sigma\kappa_{\rm P}(T_s) \gg 1 , \\ \dfrac{\Sigma\kappa_Q^2(T_s)}{\kappa_{\rm P}(T_s)} & \text{for } \Sigma\kappa_{\rm P}(T_s) \ll 1 , \end{cases} \tag{A6}$$

where κ_Q is the Planck square mean opacity

$$\kappa_Q^2(T) \equiv \frac{\int_0^\infty B_\nu(T)\kappa_\nu^2 d\nu}{\int_0^\infty B_\nu(T)d\nu} . \tag{A7}$$

To a certain degree of accuracy the approximation $\kappa_Q^2(T_s)/\kappa_{\rm P}(T_s) \simeq \kappa_{\rm P}(T_s)$ can be used.

When the above limiting expressions for ψ_s (eq. [A6]) and ψ_i (eq. [A3]) are inserted into equation (4), then one reproduces equations (12a), (12b), and (12c) of CG97.

Since these ψ_i and ψ_s depend on T_i itself (the determination of which requires the values of ψ_i and ψ_s), the solution of equation (4) requires an iterative procedure.

A2. THE $\chi_{\rm cg}$ PARAMETER

For a given grazing angle α, the ratio $\chi_{\rm cg} \equiv H/h$ is independent of h. However, α itself depends on H through equation (1). We define H to be the height at which

$$\frac{\kappa_{\rm P}(T_*)}{\alpha} \int_H^\infty \rho(z)dz = 1 . \tag{A8}$$

Since the vertical density distribution is assumed to be a Gaussian, this amounts to solving the following equation:

$$1 - {\rm erf}\left(\frac{\chi_{\rm cg}}{\sqrt{2}}\right) = \frac{2\alpha(\chi_{\rm cg})}{\Sigma\kappa_{\rm P}(T_*)} , \tag{A9}$$

where, for a given value of h, the α depends on $\chi_{\rm cg}$ through equation (1). Equation (A9) can be quickly solved for $\chi_{\rm cg}$ using any kind of root-finding algorithm.

A3. THE $\chi_{\rm rim}$ PARAMETER

In this section we wish to determine the dimensionless parameter $\chi_{\rm rim} = H_{\rm rim}/h_{\rm rim}$, which determines the vertical height of the inner rim. We define the surface height to be the height to which the optical depth of the rim on a radially outward directed ray is greater than 1:

$$\tau_r(z_0) = \int_{R_{\rm rim}}^\infty \rho(R, z)\kappa_{\rm P}(T_*)dR = 1 , \tag{A10}$$

where $z = z_0 R$ and z_0 is the value of z at $R = R_{\rm rim}$. We neglected a geometric factor $(1 + z_0^2/R_{\rm rim}^2)^{1/2}$ (arising from cylindrical coordinates) because it is very close to unity.

In order to determine $\tau_r(z_0)$, we need to know the two-dimensional structure of the puffed-up inner rim, which we discussed in § 2.3. We have estimated the radial behavior of $H(R)/R$ to be linear with a slope of $-\frac{1}{8}$. A radial ray through the upper layers of the inner edge will therefore have a roughly 8 times higher optical depth than a vertical ray between $z = z_0$ and

$z = \infty$. In order to estimate z_0, we therefore estimate $\tau_r(z_0)$ to be simply 8 times $\tau_v(z_0)$:

$$\tau_r(z_0) = 8\int_z^\infty \rho(R_{\rm rim}, z)\kappa_{\rm P}(T_*)dz' = \frac{8\Sigma\kappa_{\rm P}(T_*)}{\sqrt{\pi}} \int_{z/h_{\rm rim}}^\infty e^{-x^2}\,dx\,, \tag{A11}$$

which can be easily computed following the procedure in § A2.

APPENDIX B

EMISSION FROM A CYLINDER

B1. FAR-FIELD LIMIT

Consider the inner rim to be a cylinder with radius $R_{\rm rim}$ and vertical height $H_{\rm rim}$, emitting toward the inside as a blackbody of temperature $T_{\rm rim}$. The unocculted surface as seen by an observer at inclination i (measured from the pole) can be computed as follows. Define the quantity δ,

$$\delta \equiv \frac{H_{\rm rim}}{R_{\rm rim}} \tan i\,, \tag{B1}$$

where δ is defined so that for $\delta = 1$ the inclination is just small enough that we are able to see the central star (which is assumed to be a point source). For $\delta < 1$ we have a more face-on view, while $\delta > 1$ means a more edge-on view of the system. The observed flux at a distance d from this cylinder in the far-field limit for $\delta < 1$ is

$$F_v = 2B_v(T_{\rm rim})\left(\frac{R_{\rm rim}}{d}\right)^2 \cos i(\delta\sqrt{1-\delta^2} + \arcsin\,\delta) \tag{B2}$$

and for $\delta > 1$ is

$$F_v = \pi B_v(T_{\rm rim})\left(\frac{R_{\rm rim}}{d}\right)^2 \cos i\,. \tag{B3}$$

B2. NEAR-FIELD LIMIT

In the far-field limit, the rim becomes invisible at $i = \pi/2$, which corresponds to $z/R = 0$. In order to compute the contribution of the inner rim to the irradiation of the flared disk, we need to correct the equation for the fact that the rim becomes invisible already at $z = H_{\rm rim}$. We do this by introducing a modified inclination θ defined by

$$\tan\theta = \frac{R - R_{\rm rim}}{z - H_{\rm rim}}\,, \tag{B4}$$

where we took the reference point to be the nearest corner of the cylinder instead of the star. We can then write δ as

$$\delta = \frac{R/R_{\rm rim} - 1}{z/H_{\rm rim} - 1}\,. \tag{B5}$$

The flux is then further given by equations (B2) and (B3). Comparing the resulting flux with exact numerical evaluation of the projected surface has shown that this approximation gives irradiation fluxes accurate to within 20% for inclinations greater than $\pi/4$ and $R > 2R_{\rm rim}$.

REFERENCES

Beckwith, S. V. W., Sargent, A. I., Chini, R. S., & Güsten, R. 1990, AJ, 99, 924
Bell, K. R. 1999, ApJ, 526, 411
Bell, K. R., & Lin, D. N. C. 1994, ApJ, 427, 987
Bouwman, J., de Koter, A., van den Ancker, M. E., & Waters, L. B. F. M. 2000, A&A, 360, 213
Calvet, N., Magris, G. C., Patino, A., & D'Alessio, P. 1992, Rev. Mexicana Astron. Astrofis., 24, 27
Calvet, N., Patino, A., Magris, G. C., & D'Alessio, P. 1991, ApJ, 380, 617
Chiang, E. I. 2000, Ph.D. thesis, California Institute of Technology
Chiang, E. I., & Goldreich, P. 1997, ApJ, 490, 368
———. 1999, ApJ, 519, 279
Chiang, E. I., Joung, M. K., Creech-Eakman, M. J., Qi, C., Kessler, E. J., Blake, G. A., & van Dishoeck, E. F. 2001, ApJ, 547, 1077
D'Alessio, P., Calvet, N., Hartmann, L., Lizano, S., & Canto, J. 1999, ApJ, 527, 893
D'Alessio, P., Canto, J., Calvet, N., & Lizano, S. 1998, ApJ, 500, 411
Draine, B., & Lee, H. M. 1984, ApJ, 285, 89
Dullemond, C. P. 2000, A&A, 361, L17
Ghandour, L., Strom, S., Edwards, S., & Hillenbrand, L. 1994, in ASP Conf. Ser. 62, The Nature and Evolutionary Status of Herbig Ae/Be Stars, ed. P. S. Thé, M. R. Pérez, & E. P. J. van den Heuvel (San Francisco: ASP), 223
Gullbring, E., Hartmann, L., Briceno, C., & Calvet, N. 1998, ApJ, 492, 323
Hartmann, L., Kenyon, S. J., & Calvet, N. 1993, ApJ, 407, 219
Herbig, G. H. 1960, ApJS, 4, 337
Hillenbrand, L. A., Strom, S. E., Vrba, F. J., & Keene, J. 1992, ApJ, 397, 613
Ivezic, Z., Groenewegen, M. A. T., Men'Shchikov, A., & Szczerba, R. 1997, MNRAS, 291, 121
Kenyon, S. J., & Hartmann, L. 1987, ApJ, 323, 714
Kenyon, S. J., Yi, I., & Hartmann, L. 1996, ApJ, 462, 439
Lada, C. J., & Adams, F. C. 1992, ApJ, 393, 278
Lin, D. N. C., & Papaloizou, J. 1980, MNRAS, 191, 37
Mannings, V., & Sargent, A. I. 1997, ApJ, 490, 792

Mannings, V., & Sargent, A. I. 2000, ApJ, 529, 391
Meeus, G., Waters, L. B. F. M., Bouwman, J., van den Ancker, M. E., Waelkens, C., & Malfait, K. 2001, A&A, 365, 476
Millan-Gabet, R., Shloerb, F. P., & Traub, W. A. 2001, ApJ, 546, 358
Natta, A. 1993, ApJ, 462, 761
Natta, A., & Krügel, E. 1995, A&A, 302, 849
Natta, A., Prusti, T., Neri, R., Grinin, V. P., & Mannings, V. 2001, A&A, 371, 186
Ruden, S. P., & Pollack, J. B. 1991, ApJ, 375, 740
Tambovtseva, L. V., Grinin, V. P., Rodgers, B., & Kozlova, O. V. 2001, Astron. Rep., 45, 442